Engineering Fracture Mechanics Vol. 35, No. 1/2/3, pp. 145–157, 1990
Printed in Great Britain.

0013-7944/90 $3.00 + 0.00
Pergamon Press plc.

MIXED MODE FRACTURE ENERGY OF CONCRETE

ENRICO BALLATORE,† ALBERTO CARPINTERI,† GERARDO FERRARA‡ and GIORGIO MELCHIORRI‡

†Department of Structural Engineering, Politecnico di Torino, 10129 Torino, Italy and
‡E.N.E.L.—C.R.I.S., 20162 Milano, Italy

Abstract—An interpretation of the very complex failure mechanism in four point shear specimens of concrete is proposed. A size-scale transition between tensile strength failure and mixed mode crack propagation is demonstrated to occur. When the distance of the central supports is large, the tensile strength is overcome at the supports by flexure. When the same distance is small, the tensile strength is overcome in the middle of the specimen by splitting. Pure shear failure does not seem to activate locally. As a matter of fact, the mixed mode fracture energy is substantially equal to the mode I fracture energy G_F, each crack growth step being produced by a mode I (or opening) mechanism.

1. INTRODUCTION

THE INTERPRETATION of the four-point shear test of concrete (Fig. 1) is rather problematic and controversial. More than one failure mechanism seems to contribute to the final collapse of such a specimen: (1) mixed mode crack propagation; (2) flexural failure on the supports; (3) tensile splitting failure in the middle of the specimen; (4) pure shear failure between the central supports; etc.[1–3]. In the present paper, it is demonstrated that a size-scale transition occurs between mechanisms (2) and (1) by increasing the beam depth, when the distance between the central supports is not too small. When such a distance is comparatively very small, the transition occurs between mechanisms (3) and (1)[1]. Mechanism (4) does not activate locally, but only globally and is always produced by local tensile stresses. The proof to this statement is provided by the mixed mode fracture energy, which is given by the total dissipated energy on the fracture surface, divided by the total fracture area. This experimental quantity is very close to the value of mode I fracture energy G_F[4]. In this investigation, the remarkable amount of energy dissipated in the volume—by punching at the supports and by compression inside the specimen—was deliberately neglected.

The experimental tests were carried out selecting two different materials and three different sizes, and applying to each case three different loading conditions. For any of these combinations the tests were reiterated four times. Each test was controlled by the crack sliding displacement or by the loading point deflections. The constitutive law of the material was defined by means of tensile testing under controlled deformation.

A numerical approach to the problem is provided by a computer code based on the Strain Energy Density Theory[5, 6]. The material damage is taken into account by a suitable reduction in the elastic modulus according to the strain energy absorbed in the element. The non-collinear crack growth is evaluated at each step and a new crack tip position is computed. The finite element core region corresponding to the crack tip area is translated and modified at each step. The crack trajectories and the load vs deflection responses are reproduced by the finite element code in a satisfactory way.

2. EXPERIMENTAL PROGRAM

2.1. *Material properties*

Two different concretes, with maximum aggregate size $D_{max} = 10$ and 20 mm respectively, were selected to carry out the Round Robin proposed by Carpinteri[3] to the RILEM Committee 89-FMT. The alluvial aggregates were subdivided into three classes and the weight composition is reported in Table 1.

The relevant mechanical properties (measured after 28 days from moulding) are provided in Table 2. Then, after the same curing time, three-point bending tests to obtain the fracture energy

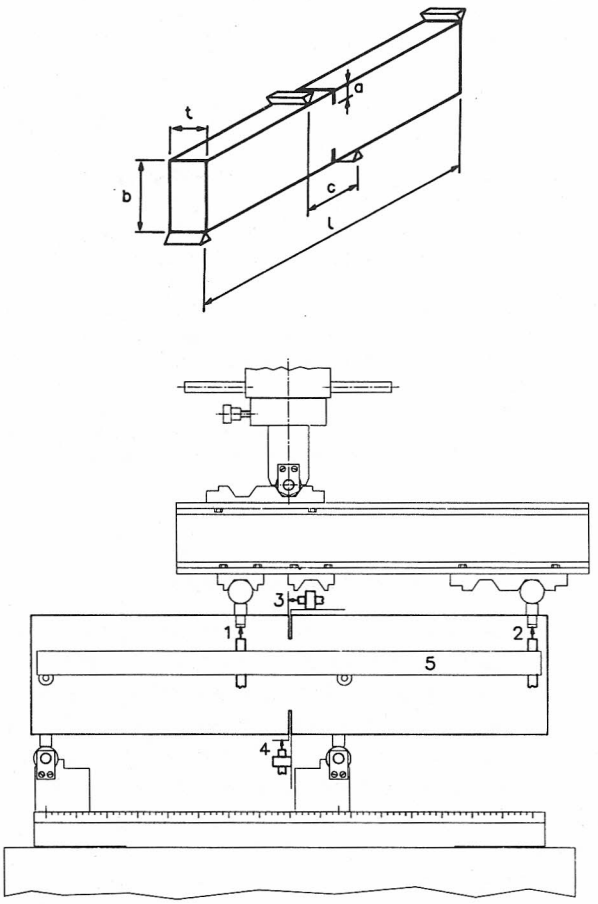

1 – LVDT for the measurement of δ_1 deflection

2 – LVDT for the measurement of δ_2 deflection

3 – LVDT for the measurement of C.M.O.D.

4 – LVDT for the measurement of C.M.S.D.

5 – Reference bar for δ_1 and δ_2 measurement

Fig. 1. Loading configuration and LVDT positions.

G_F were carried out, according to the RILEM Recommendation[4]. The same fracture toughness parameter was determined also by stable direct tension tests on prenotched cylindrical specimens of diameter $\phi = 10$ cm and height $H = 20$ cm. The related experimental results, averaged over four (4) identical specimens, are reported in Table 3.

Table 1. Concrete mix proportions

Composition		Concrete 1	Concrete 2
H.R. Portland Cement		460 kg/m^3	400 kg/m^3
Water		210 kg/m^3	180 kg/m^3
Aggregate	Sand 0–3	672 kg/m^3	546 kg/m^3
	Sand 3–10	1008 kg/m^3	728 kg/m^3
	Gravel 10–20	—	546 kg/m^3
Water/cement ratio		0.457	0.450
Aggregate maximum size		10 mm	20 mm

Table 2. Mechanical properties of concrete

Properties	Concrete 1	Concrete 2
Compression test on cubic specimen $10 \times 10 \times 10$ cm σ_c (kg/cm^2)	507	530
Direct tensile test on specimen $10 \times 10 \times 21$ cm σ_u (kg/cm^2)	21.4	24.7
Young's modulus, compression on specimen $10 \times 10 \times 30$ cm E (kg/cm^2)	358,000	379,000

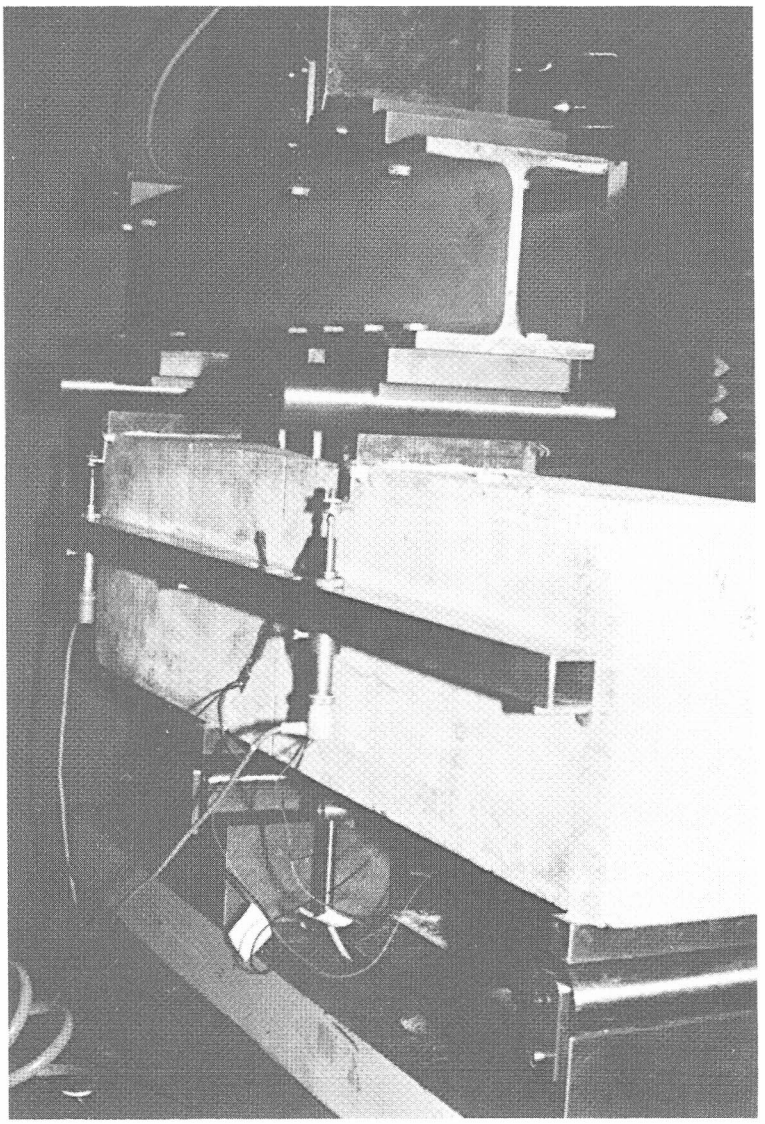

Fig. 2. Experimental apparatus. Detail of the reference bar for δ_1 and δ_2 measurement.

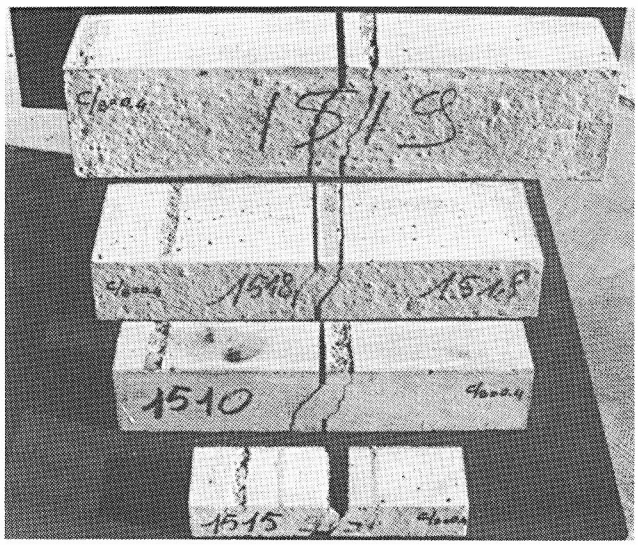

2B/0.4

2A/0.4

1B/0.4

1A/0.4

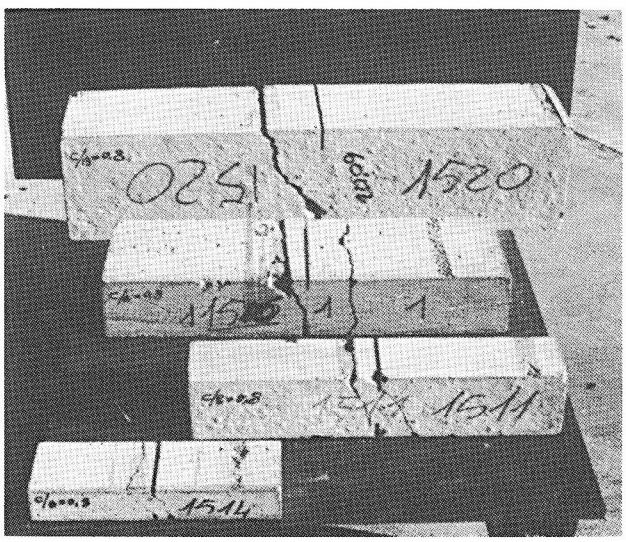

2B/0.8

2A/0.8

1B/0.8

1A/0.8

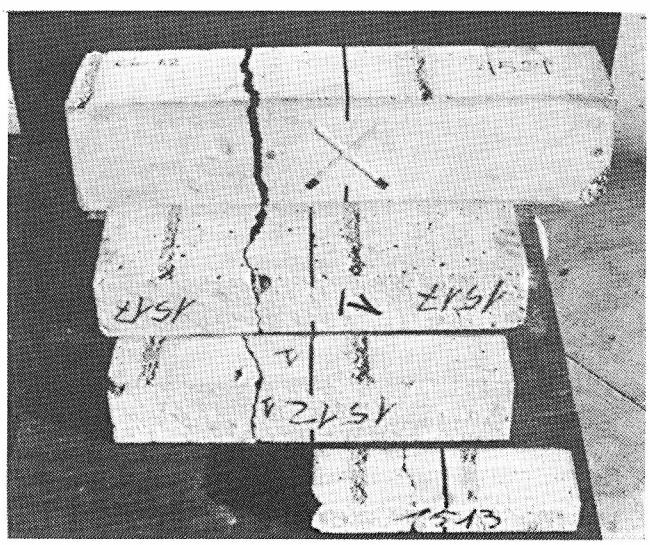

2B/1.2

2A/1.2

1B/1.2

1A/1.2

Fig. 3. Different failure mechanisms for each c/b ratio of selected specimen geometries.

Table 3. Fracture energy G_F

Testing procedure	Specimen sizes	Concrete	Fracture energy G_F (N/m)
Stable three-point bending test (T.P.B.T.)	$10 \times 10 \times 84$ cm	1	131.1 ± 19.6
		2	126.4 ± 18.9
Stable tension test	$\phi = 10$, $H = 20$ cm	1	92.9 ± 14.45
		2	97.9 ± 2.33

The fracture energy provided by the three-point bending test appears higher than that provided by the direct tension test. This is due to the additional energy dissipated by punching at the supports and by compression at the upper beam edge. Moreover, the standard deviation is lower in the case of direct tension test, the energy dissipation zone being more evident and localized.

2.2. *Four point shear specimens and experimental apparatus*

The sizes of the 64 four-point shear specimens are reported in Table 4. They are proportional to the maximum aggregate size of the two concretes. The specimens were kept in a controlled environment at 20°C and 95% relative humidity up to four hours before testing. The notches were performed by means of a circular saw. Each specimen was provided with four supports of sizes $2 \times 2 \times 20$ cm, glued at the four intended loading points, and with displacement transducers (LVDT) to measure crack mouth opening displacement (CMOD) and crack mouth sliding displacement (CMSD).

The testing configuration is that shown in Fig. 1. An I-beam was interposed between testing machine (max. load = 20 t) and specimen, in order to distribute the load (Fig. 2). The first set of tests (specimens 1B/0.4 and 1B/0.8) were CMSD-controlled with an imposed rate of 0.025 μm/s. Remarkable noise and anomalies in the measurement of CMSD and CMOD were noticed for $c/b > 0.4$, and made the testing control difficult. Therefore, the average value of the two loading point deflections, δ_1 and δ_2, was selected as feed-back signal (Fig. 1). In this way, the testing procedure resulted to be stable, although the CMSD and CMOD records were still very irregular, specially for $c/b = 0.8$ and 1.2. The results are displayed in Tables 5 and 6, for concrete 1 and 2, respectively. In addition to the failure load, even the failure mechanism is described, indicating with MM, the mixed mode cracking, and with FLEX, the flexural failure at the support.

The photographs in Fig. 3 show the different failure mechanisms, for each c/b ratio selected for the experimental investigation. It is remarkable that, for $c/b = 0.4$, the failure mechanism was mixed mode cracking in any case, whereas, for $c/b = 1.2$, it was always due to flexure at the

Table 4. Testing geometries

D_{max} (mm)	Specimen	Depth b (cm)	Thickness $t = 10 \times D_{max}$ (cm)	Span $l = 4b$ (cm)	Crack length $a = 0.2 \times b$ (cm)	c (cm)	c/b
10	1A/0.4	5	10	20	1	2	0.4
	1A/0.8					4	0.8
	1A/1.2					6	1.2
	1B/0.2	10	10	40	2	2	0.2
	1B/0.4					4	0.4
	1B/0.8					8	0.8
	1B/1.2					12	1.2
	1C/0.4	20	10	80	4	8	0.4
	1C/0.8					16	0.8
	1C/1.2					24	1.2
20	2A/0.4	10	20	40	2	4	0.4
	2A/0.8					8	0.8
	2A/1.2					12	1.2
	2B/0.4	20	20	80	4	8	0.4
	2B/0.8					16	0.8
	2B/1.2					24	1.2

Table 5. Experimental results for concrete 1

Specimen	c (cm)	Maximum load P_{max} (kg)	Maximum load average P_{max} (kg)	Failure mechanism
1A/0.4	2	2137 2023 1988 2295	2110.8 ± 138.3	MM**
1A/0.8	4	1795 1689 1901	1795.0 ± 106.0	MM**
1A/1.2	6	1650 1606	1628.0 ± 31.1	FLEX
1B/0.2	2	3300 3980 3425	3578.8 ± 296.3	MM**
1B/0.4	4	3610 3390 3330 2876 3336	3233.0 ± 239.5	MM**
1B/0.8	8	3658 3746 3522 3272	3549.5 ± 206.7	MM* MM** MM** MM*
1B/1.2	12	3570 2958 2918 3050	3124.0 ± 302.4	FLEX
1C/0.4	8	6100 5580 5840 5920	5860.0 ± 216.0	MM*
1C/0.8	16	6120 6240 5760	6040.0 ± 249.8	MM* MM* MM*
1C/1.2	24	4600 3840 5080 4400	4480.0 ± 513.3	FLEX

MM* = Mixed-mode cracking (one surface).
MM** = Mixed-mode cracking (two surfaces).
FLEX = Flexural failure.

Table 6. Experimental results for concrete 2

Specimen	c (cm)	Maximum load P_{max} (kg)	Maximum load average P_{max} (kg)	Failure mechanism
2A/0.4	4	7740 7848 8950 8224	8190.5 ± 547.2	MM**
2A/0.8	8	7595 6816 7384 6420	7053.8 ± 535.5	MM*
2A/1.2	12	6472 6248 6404 5828	6238.0 ± 289.0	FLEX
2B/0.4	8	11,280 12,240 12,400	11,973.3 ± 605.8	MM* MM** MM**
2B/0.8	16	11,040 10,440 10,660 10,880	10,755.0 ± 261.5	MM* FLEX MM* MM*
2B/1.2	24	8340 9040 9040 9460	8970.0 ± 464.3	FLEX

MM* = Mixed-mode cracking (one surface).
MM** = Mixed-mode cracking (two surfaces).
FLEX = Flexural failure.

support. On the other hand, the case $c/b = 0.8$ seems to represent a transition between the two mechanisms previously considered.

Only for some specimens (1B/0.2, 1C/0.4, 1C/0.8) the displacement signals related to the two loading points, δ_1 and δ_2, were separated. For these cases, it was then possible to record the diagrams F_1–δ_1 and F_2–δ_2, F_1 and F_2 being the two forces acting onto the specimen (Fig. 4). When the crack propagation occurs only from one notch (due to the asymmetry of the specimen weight), the diagram F_1–δ_1 presents elastic unloading (Fig. 4b).

The fracture trajectories on the single specimen sides were recorded, for all the cases undergoing mixed mode cracking. The single and average trajectories are drawn in Fig. 5(a and b), respectively for specimens 2A/0.4 and 2B/0.4.

3. NUMERICAL SIMULATION

A computer code was developed in order to simulate mixed mode crack propagation. The material constitutive model adopted in the code is based on the assumption of bilinear

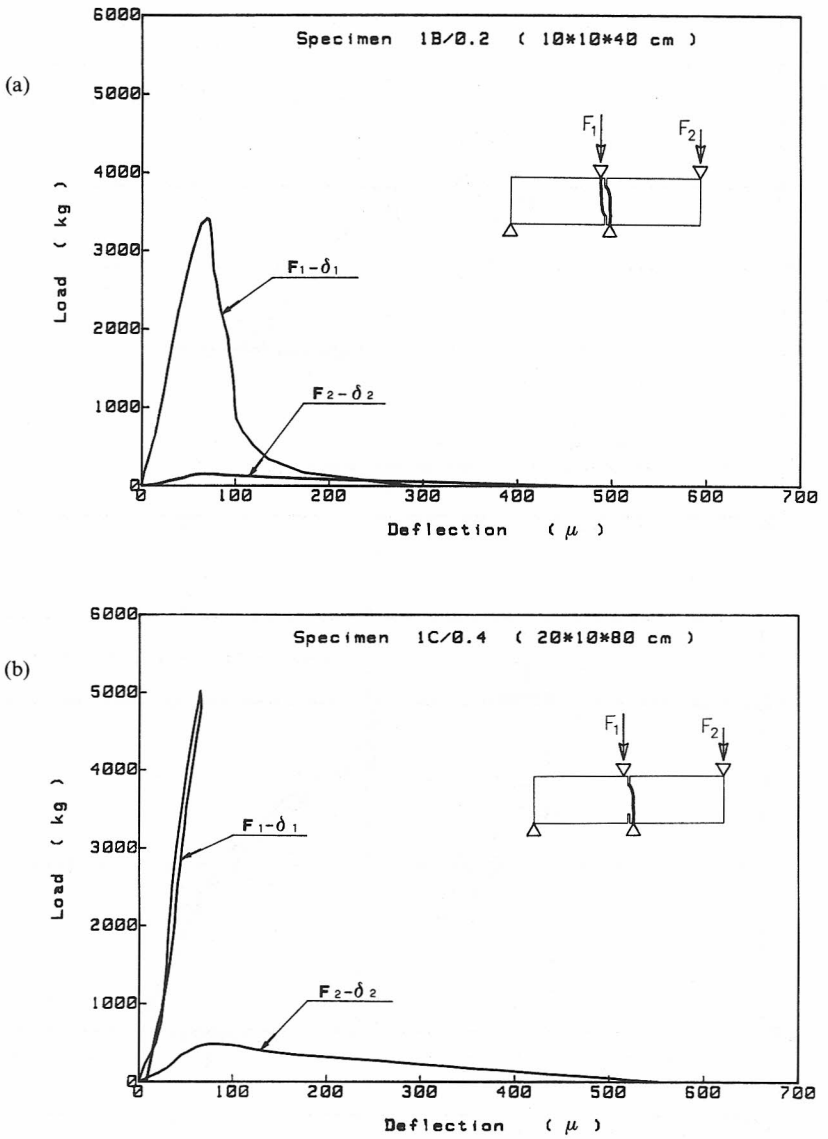

Fig. 4. (a) Load vs deflection diagrams related to the two loading points (specimen 1B/0.2). (b) Load vs deflection diagrams related to the two loading points (specimen 1C/0.4).

elastic-softening stress–strain variation (Fig. 6), and used to determine the decrease of elastic modulus due to mechanical damage. On the other hand, the crack growth step is evaluated according to the strain energy density accumulated in the crack tip vicinity[5, 6]. The code, whose previous version simulates only mode I crack propagation, is composed by:

(1) The program APES, which utilizes 12-noded quadrilateral isoparametric finite elements allowing for cubic displacement fields and quadratic stress and strain fields within any element;

(2) The program DAMG, which reduces the effective elastic modulus E^* to be assigned to each element for the evaluation of the damage effect at each step;

(3) The program CKGW, which computes the crack growth increment at each step on the basis of the Strain Energy Density Theory;

(4) The program MESH, which modifies and updates the finite element mesh at each step in order to reproduce the fracture trajectory.

The numerical simulation of the F_1–δ_1 and F_2–δ_2 curves of specimen 1C/0.8 is shown in Fig. 7. The crack propagation occurred only from one notch (due to the asymmetry of the specimen weight), so that the experimental diagram F_1–δ_1 presents elastic unloading (see also Fig. 4b). The

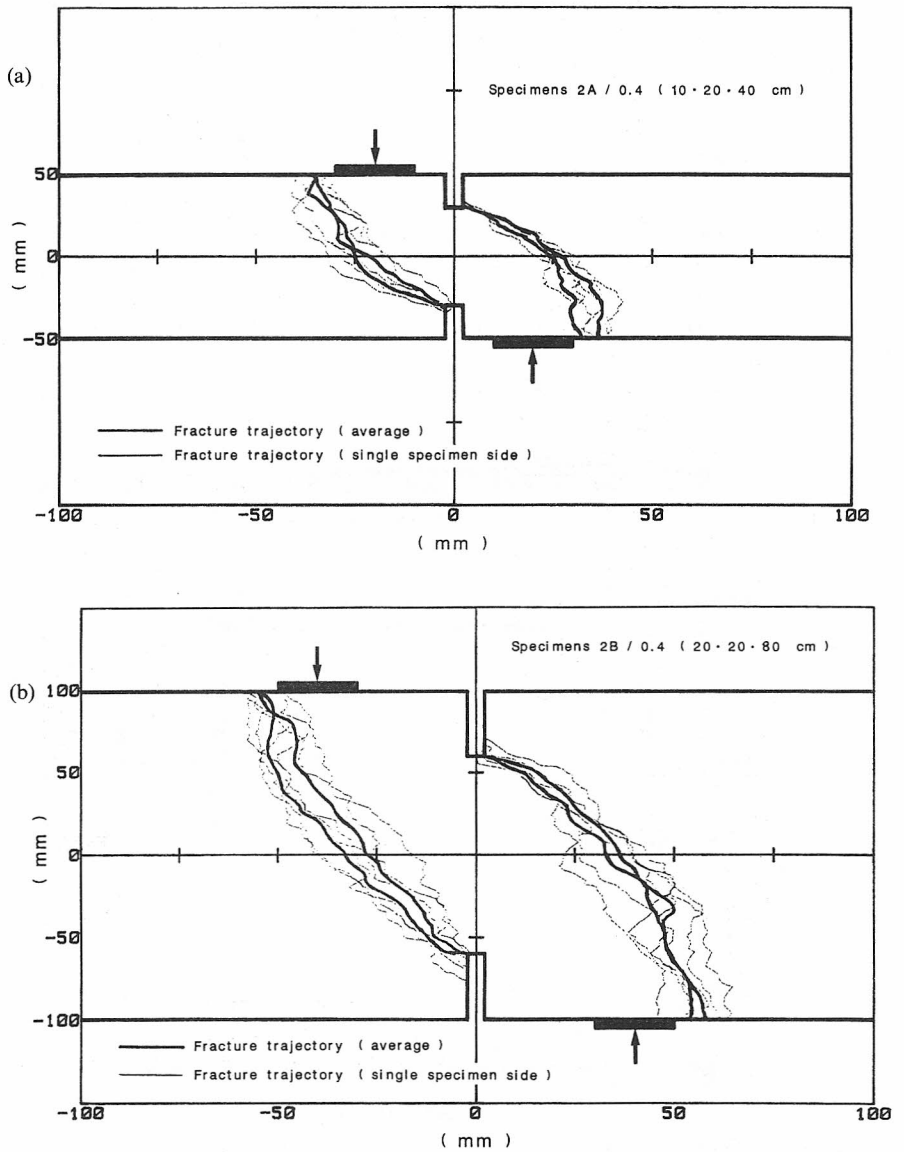

Fig. 5. (a) Fracture trajectories (specimen 2A/0.4). (b). Fracture trajectories (specimen 2B/0.4).

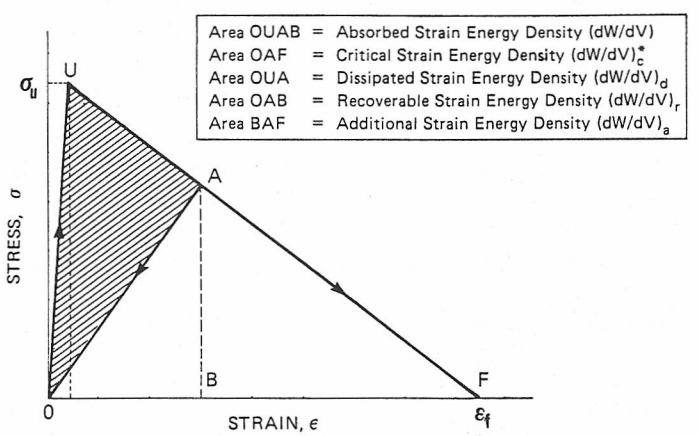

Fig. 6. Stress–strain elastic-softening diagram.

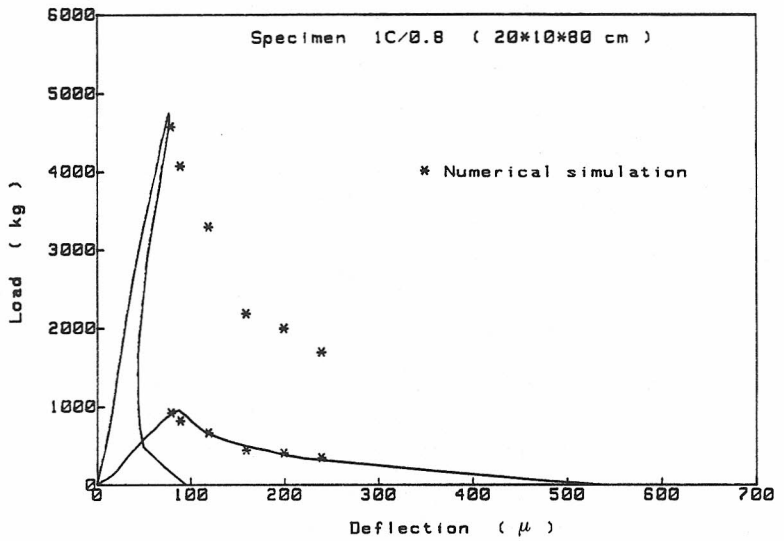

Fig. 7. Load–deflection diagrams for specimen 1C/0.8. Comparison between experimental and numerical results.

numerical simulation takes into account, on the other hand, two symmetrical crack trajectories, one of which, in practice, did not develop. In this way, even the diagram F_1–δ_1 would reveal a softening behaviour, as always in practice does the diagram F_2–δ_2. The loading process was simulated by imposing six (6) consecutive steps to the loading point deflection. If the asymmetry due to specimen weight and material inhomogeneity is neglected, the deflections δ_1 and δ_2 are the same.

The material properties utilized in the numerical analysis are given in Table 2. The fracture strain ϵ_f (Fig. 6) can be obtained from the expression[6,7]:

$$\epsilon_f = \frac{2G_F/\sigma_u}{3D_{max}}. \tag{1}$$

In the numerical analysis the value $\epsilon_f = 2.58 \times 10^{-3}$ was assumed for concrete 1.

The sequence of the six (6) finite element meshes, updated and modified after each loading step, is plotted in Fig. 8. The deformed four-point shear specimen configuration at the 6th step is displayed in Fig. 9.

4. MIXED MODE SIZE EFFECT

From the experimental results it comes out that there are two potential failure mechanisms in competition, by varying the support distance c (Table 4) as well as by varying the size-scale b of the four-point shear specimen. Mixed mode crack propagation is favoured for small distances c and/or for large sizes b. On the contrary, flexural failure at the supports is favoured for large distances c and/or for small sizes b. Ingraffea and Panthaki[1] argued about a third failure mechanism which activates for very small distance c: the splitting ultimate strength at the centre of the specimen. It is remarkable that all the three failure mechanisms may be imputed to tensile stress, and not to local shear deformations[2].

As a matter of fact, by increasing the size-scale of a concrete element, the influence of heterogeneity disappears and the body may be considered as macroscopically homogeneous. Moreover, by increasing the size-scale of a cracked concrete element, the influence of the non-linear softening material behaviour vanishes, the cohesive crack tip forces disappear and the crack propagation is governed only by the linear elastic stress-singularity in the crack tip region[8, 9]. This means that LEFM is a valid crack branching criterion for large concrete structures. For mode I crack propagation, this has already been demonstrated[7–8, 11–15]. For mixed mode crack propagation, this is a logical consequence, since the mode II stress-singularity power is still 1/2 as for mode I.

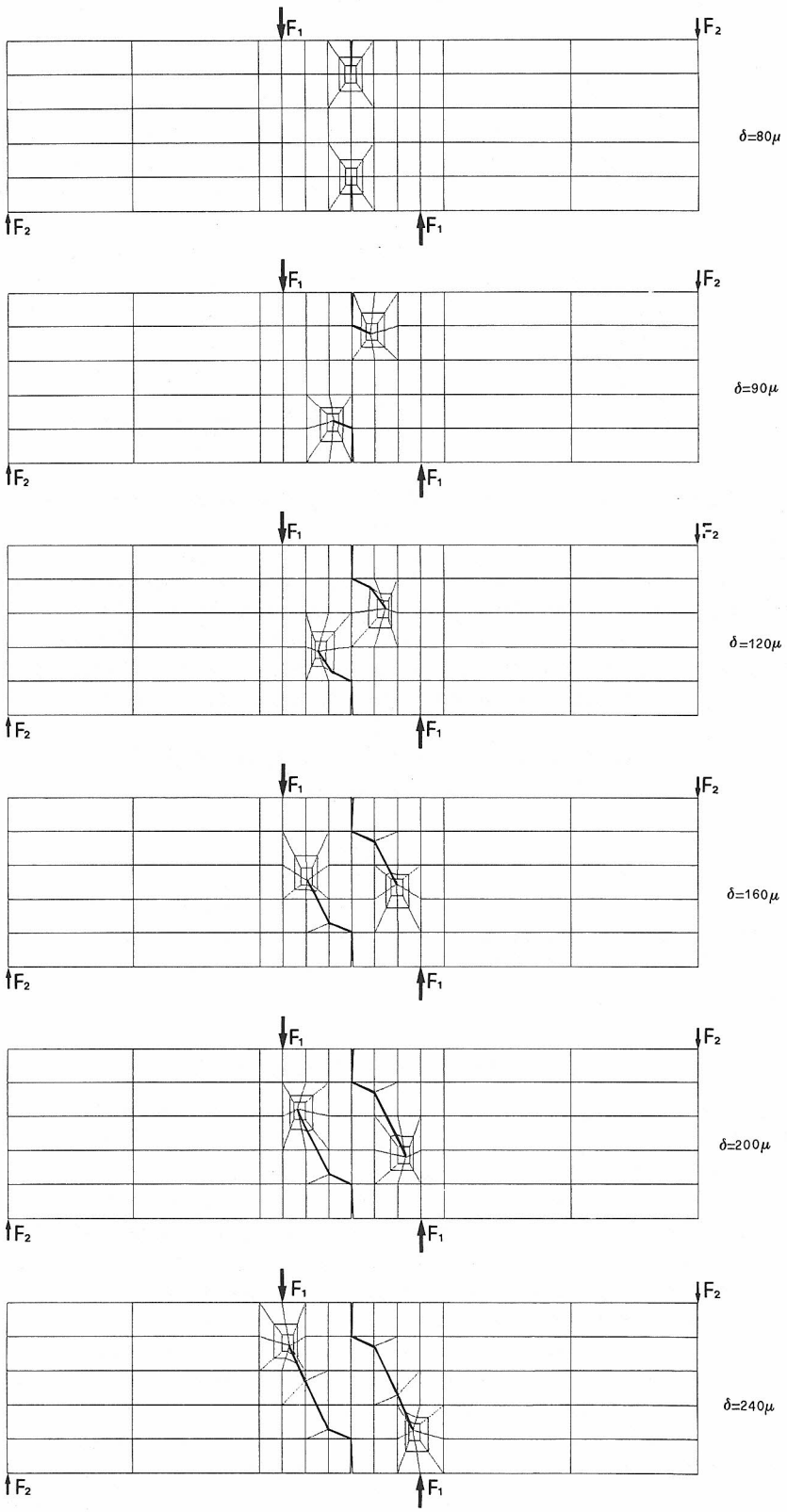

Fig. 8. Finite element meshes for the six different loading steps.

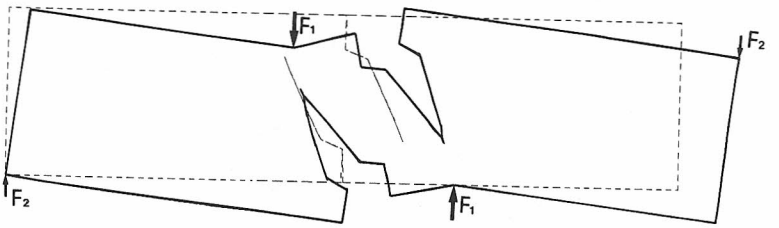

Fig. 9. Deformed specimen configuration at the 6th loading step.

In the four-point shear test, stress intensification is produced in both the crack tip regions and the stress-intensity factors for mode I and mode II can be expressed respectively as:

$$K_{\mathrm{I}} = \frac{P}{tb^{1/2}} f_{\mathrm{I}}\left(\frac{l}{b}, \frac{a}{b}, \frac{c}{b}\right), \tag{2a}$$

$$K_{\mathrm{II}} = \frac{P}{tb^{1/2}} f_{\mathrm{II}}\left(\frac{l}{b}, \frac{a}{b}, \frac{c}{b}\right), \tag{2b}$$

where P is the total load and f_{I}, f_{II} are the shape functions.

Most relevant mixed mode fracture criteria can be expressed in the approximate form:

$$K_{\mathrm{I}}^2 + q^2 K_{\mathrm{II}}^2 = K_{\mathrm{IC}}^2 = G_{\mathrm{F}} E, \tag{3}$$

where q is a measure of the influence of mode II on crack branching. Equations (2) and (3) provide:

$$\frac{P_{\max}}{tb^{1/2}} = \frac{K_{\mathrm{IC}}}{\sqrt{f_{\mathrm{I}}^2 + q^2 f_{\mathrm{II}}^2}}. \tag{4}$$

If the geometric ratios l/b and a/b are constant, eq. (4) becomes:

$$\frac{P_{\max}}{\sigma_{\mathrm{u}} tb} = \frac{s}{F\left(\frac{c}{b}\right)}, \tag{5}$$

where s is the brittleness number[10, 11]:

$$s = \frac{K_{\mathrm{IC}}}{\sigma_{\mathrm{u}} b^{1/2}}. \tag{6}$$

On the other hand, the bending tensile stress at the supports is:

$$\sigma = 3P \frac{c(l-c)}{tb^2(l+c)}. \tag{7}$$

The maximum load due to the formation of a plastic cohesive hinge[9] at the support is given in dimensionless form:

$$\frac{P_{\max}}{\sigma_{\mathrm{u}} tb} = \frac{4 + \frac{c}{b}}{\frac{c}{b}\left(4 - \frac{c}{b}\right)}. \tag{8}$$

Equations (5) and (8) are in competition by varying the value of the brittleness number s or the ratio c/b. If the latter is fixed, there is a size-scale transition which is described in Fig. 10. The experimental results of the present research are reported in Fig. 11 where the maximum load divided by the beam area is plotted against the inverse root $b^{-1/2}$. The experimental points describe the transition between an inclined straight line and a horizontal asymptote. The former represents the LEFM instability, whereas the latter the ultimate bending strength at the supports (Fig. 11a). Concrete 2 appears brittler than concrete 1, the horizontal asymptote being absent in Fig. 11(b).

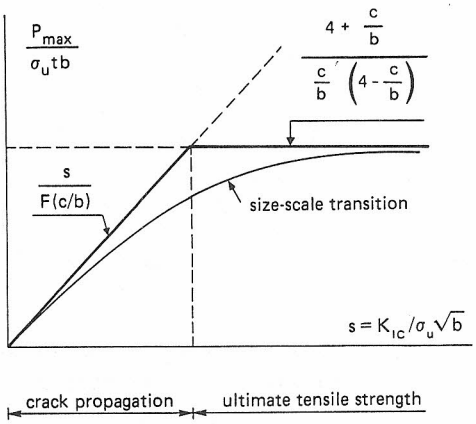

Fig. 10. Size-scale transition. Maximum load vs brittleness number.

5. MIXED MODE FRACTURE ENERGY

The energy dissipated by testing specimens 1B/0.2, 1C/0.4 and 1C/0.8, is reported in Table 7. W_1 and W_2 represent the work done by force F_1 and force F_2 respectively:

$$W_i = \int_0^{\delta_{0i}} F_i \, d\delta_i, \quad i = 1,2. \tag{9}$$

W_1 is zero for specimen 1C, where only one crack developed and dissipated surface energy. W_2 is different from zero in any case. The total dissipated energy W_0 is obtained by summation of W_1 and W_2. The only specimen where both the cracks propagated at the same time was 1B/0.2. The total area of the curved fractures is provided in Table 6, as well as the mixed mode fracture energy, which, by definition, is the ratio of the energy W_0 to the total fracture area. It is interesting to observe that the mixed mode fracture energy results to be of the same order of magnitude of mode I fracture energy G_F. For specimen 1B/0.2 it appears higher than G_F, probably due to additional energy dissipated in the volume of the specimen. On the other hand, it appears slightly lower than G_F for specimens 1C/0.4 and 1C/0.8, probably because the work done by the specimen weight was neglected.

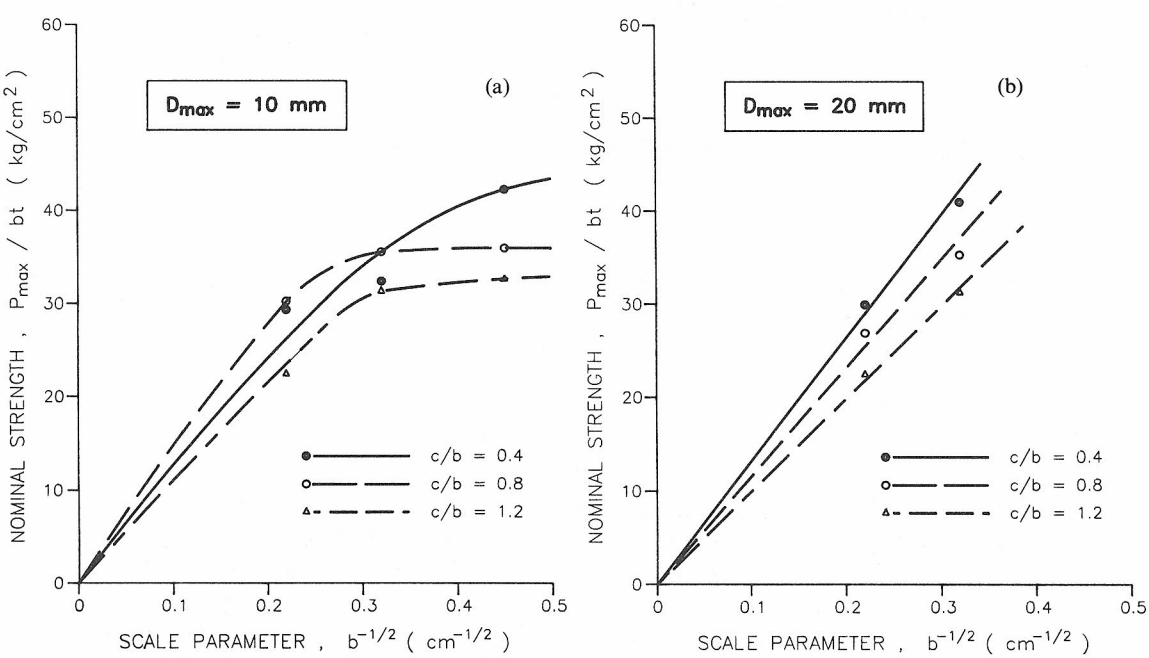

Fig. 11. (a) Size-scale transition from LEFM instability to tensile strength collapse (concrete 1). (b) Size-scale transition from LEFM instability to tensile strength collapse (concrete 2).

Table 7. Comparison between mixed-mode fracture energy and mode I fracture energy

Specimen	W_1 (Nm)	W_2 (Nm)	$W_0 = W_1 + W_2$ (Nm)	Failure mechanism	Total fracture area (m^2)	Mixed-mode fracture energy (N/m)	Mode I fracture energy G_F (N/m)
1B/0.2	2.40	0.34	2.74	MM**	0.0184	148.9	
		1.55	1.55		0.0184	84.2	
1C/0.4	0.00	1.28	1.28	MM*	0.0193	66.3	92.9
		1.49	1.49		0.0190	78.4	
		1.29	1.29		0.0203	63.5	
1C/0.8	0.00	1.61	1.61	MM*	0.0200	80.5	
		1.74	1.74		0.0200	87.0	

$W_1 = \int F_1 \, d\delta_1$ MM* = Mixed-mode cracking (one surface).
$W_2 = \int F_2 \, d\delta_2$ MM** = Mixed-mode cracking (two surfaces).

From the comparison between mixed mode fracture energy and mode I fracture energy G_F, it comes out that:

(1) Each crack propagation step is always produced by a mode I (opening) mechanism;
(2) The fracture toughness of concrete is defined by the unique parameter G_F, even for mixed mode problems.

Acknowledgements—The results reported in the present paper were obtained in a joint research program between ENEL-CRIS-Milano and Politecnico di Torino.

REFERENCES

[1] A. R. Ingraffea and M. J. Panthaki, Analysis of shear fracture tests of concrete beams. *Seminar on Finite Element Analysis of Reinforced Concrete Structures*, May 21–24, 1985, Tokyo, Japan, pp. 71–91 (1985).
[2] Z. P. Bažant and P. A. Pfeiffer, Shear fracture tests of concrete. *Mater. Struct.* **19,** 111–121 (1986).
[3] A. Carpinteri, Interaction between tensile strength failure and mixed mode crack propagation in concrete. Report to the RILEM Committee 89-FMT (March 1987).
[4] RILEM-Draft Recommendation, Determination of the fracture energy of mortar and concrete by means of three-point bend tests on notched beams. *Mater. Struct.* **18,** 285–290 (1985).
[5] A. Carpinteri and G. C. Sih, Damage accumulation and crack growth in bilinear materials with softening. *Theor. Appl. Fracture Mech.* **1,** 145–160 (1984).
[6] A. Carpinteri, *Mechanical Damage and Crack Growth in Concrete*. Martinus Nijhoff, Dordrecht (1986).
[7] Z. P. Bažant, Size effect in blunt fracture: concrete, rock, metal. *J. Engng Mech.* (A.S.C.E.) **110,** 518–535 (1984).
[8] A. Carpinteri, Interpretation of the Griffith instability as a bifurcation of the global equilibrium, in *Application of Fracture Mechanics to Cementitious Composites*, N.A.T.O.-A.R.W., Sept. 4–7, 1984, Northwestern University (Edited by S. P. Shah), pp. 287–316. Martinus Nijhoff, Dordrecht (1985).
[9] A. Carpinteri, Size effects on strength, toughness and ductility. To appear in *J. Engng Mech.* (A.S.C.E.).
[10] A. Carpinteri, Static and energetic fracture parameters for rocks and concretes. *Mater. Struct.* **14,** 151–162 (1981).
[11] A. Carpinteri, Notch sensitivity in fracture testing of aggregative materials. *Engng Fracture Mech.* **16,** 467–481 (1982).
[12] P. E. Petersson, Crack growth and development of fracture zones in plain concrete and similar materials. Report TVBM-1006, Division of Building Materials, Lund Institute of Technology, Sweden (1981).
[13] A. Carpinteri, A. Di Tommaso and M. Fanelli, Influence of material parameters and geometry on cohesive crack propagation, in *Fracture Toughness and Fracture Energy of Concrete*, Oct. 1–3, 1985, Lausanne (Edited by F. H. Wittmann), pp. 117–135. Elsevier, Amsterdam (1986).
[14] M. Wecharatana and S. P. Shah, Prediction of nonlinear fracture process zone in concrete. *J. Engng Mech.* (A.S.C.E.) **109,** 1231–1246 (1983).
[15] A. R. Ingraffea, Non-linear fracture models for discrete crack propagation, in *Application of Fracture Mechanics to Cementitious Composites*, N.A.T.O.-A.R.W., Sept. 4–7, 1984, Northwestern University (Edited by S. P. Shah), pp. 247–285. Martinus Nijhoff, Dordrecht (1985).

(*Received for publication* 16 *November* 1988)